

Evaluating the Influence of Quantum Noise on Different Perspectives of Quantum Image State Preparation Protocols

Megala S^{1,*}, Ragukumar P^{2,**}, and Neelu Khare^{3,***}

¹Department of Mathematics, Vellore Institute of Technology, Vellore, 632 014, Tamil Nadu, India.

²Department of Mathematics, Vellore Institute of Technology, Vellore, 632 014, Tamil Nadu, India.

³Department of Software and Systems Engineering, Vellore Institute of Technology, Vellore, 632 014, Tamil Nadu, India.

Abstract.

Quantum Image Processing is based on principles of quantum computing to represent visual information effectively, preparation of a quantum state plays a crucial role in circuit performance. In Noisy Intermediate-Scale Quantum (NISQ) era, quantum noise and decoherence predominantly affect the fidelity of image-encoded quantum states. This paper deals with a comparative analysis of Four quantum image encoding schemes namely, Flexible Representation of Quantum Images (FRQI), Quantum Probability Image Encoding (QPIE), Order-Encoded Quantum Image Model (OQIM), and Enhanced Flexible Representation of Quantum Images (EFRQI). Noise free and Noisy state preparation simulations are executed using gate-based quantum simulators in the PennyLane environment, incorporating Bit Flip (BF), Phase Flip (PF), Amplitude Damping (AD), Phase Damping (PD), and Depolarizing noise (DN) channels. Image related performance metrics such as, Mean Squared Error (MSE), Peak Signal-to-Noise Ratio (PSNR) in dB, Structural Similarity Index Measure (SSIM), and Intersection over Union (IoU) are used to measure the performance of image encoded quantum states. Our results reveal that distinct noise robustness characteristics' across various encoding methods reveals the importance of Noise aware encoding selection for NISQ era quantum image processing applications.

1 Introduction

The field of quantum computing originated from the pioneering work of Richard P. Feynman [3], who observed that classical computers face exponential computational overhead when simulating quantum systems. This fundamental limitation inspired him to propose using quantum mechanical systems themselves for computation, laying the groundwork for modern quantum computing and the development of quantum algorithms. In recent years, quantum computing has progressed significantly, with algorithms being developed for diverse applications such as optimization, cryptography, and machine learning [7]. Among these advancing areas, Quantum Image Processing (QIP) has a considerable attention due to its potential to

*e-mail: megala.s2023@vitstudent.ac.in

**e-mail: ragukumar.p@vit.ac.in, Corresponding author

***e-mail: neelu.khare@vit.ac.in

employ the fundamental quantum mechanical properties involving superposition, entanglement, and quantum parallelism to achieve computational gain in image processing tasks such as edge detection, segmentation, and computer vision [14].

Other most notable ones include image encoding in quantum hardware, there are different images encoding algorithms perspectives of quantum image encoding algorithms. Includes FRQI [6], QPIE [14], OQIM [13] and EFRQI [8]. The methods differ in terms of encoding schemes, qubit requirements, circuit complexity and image recovery properties. For a $2^n \times 2^n$ image, FRQI requires $2n + 1$ qubits and supports approximate image reconstruction, while both OQIM and EFRQI require $2n + 2$ qubits. QPIE encodes image information using $\lceil \log(r \cdot c) \rceil$ qubits, where r and c denote the number of image rows and columns, respectively, and also yields approximate retrieval.

Parallel to the domain of QIP, the main advancing framework involves Quantum Machine Learning (QML), this address the challenges related with complex high dimensional datasets and computationally complex training such as pattern recognition and related applications [2]. However in the current quantum devices work in NISQ era, this characterized by limited number of qubit counts, short coherence times and highly sensitive to environment noise and gate errors [10]. As a notable thing is there are many theoretical advancement in quantum algorithms, but they remain unsuitable for practical usage on near-term quantum hardware [4]. Quantum noise can occur from the even a small environmental interactions, measurement errors, imperfect control operations and others, this leading to decoherence effect and degradation of quantum state fidelity [1].

These noise effects creates a major problem for both quantum hardware execution and reliable simulation of developing quantum algorithms [10]. Recently many researchers can implements quantum algorithms in QML and measuring the algorithm performance by use of the complex valued state vectors in quantum circuit by Noise free truth fact simulator. However, in practice quantum hardware has the noise difficulties. So the characterization and comprehension of the effects of noise on quantum circuits is of significance in the context of noise resistant algorithms developed to implement near term quantum applications.

There are many Noise types have been proposed to capture different type of physical error mechanisms, including BF, PF, AD, PD, and DN channels [9]. Among these types of quantum noise depolarizing noise is commonly used to design isotropic errors and all of these noise models are represented by Kraus operators constructed from Pauli matrices X , Y , and Z [9]. By these different types of noise models can enables the systematic evaluation of algorithmic robustness under the realistic working conditions. Various types of Noise have been suggested to model various types of physical error mechanisms such as BF, PF, AD, PD, as well as DN channels, and many others, have been proposed to model these different kinds of physical error mechanisms of interest [9]. In this category of quantum noise depolarizing noise that is typically used to design isotropic errors and all of such noise models are described by Kraus operators as Pauli matrices, X , Y , and Z . By such a variety of noise models can make the systematic analysis of the algorithm robustness possible in the conditions of the realistic way.

2 Motivation and Contribution

The role of quantum noise has recently been explored in some situations. Winderl et al. [12] analyzed the impact of depolarizing noise on the adversarial robustness of quantum neural networks and established that noise generally reduce the classification accuracy without improving robustness in multi-class cases. In [5], a modified depolarization channel using reduced Kraus operators was proposed to lower computational overhead while preserving equivalent noise behavior. In depth analysis of the comprehensive comparative analysis of

quantum noise channels with the impact on circuit fidelity and performance was presented in [1], highlighting the necessity of noise-aware quantum circuit design.

Despite these progresses a systematic and comparative study of how different types of quantum noise channels can affect quantum image encoding during state preparation study remains limited. Every QML algorithms, the input to the quantum circuit for ansatz is crucial, as the performance and feature learning of the model is highly depends on the input encoding stage. In this study, we focus on this crucial component by evaluating the effect of applying quantum noise to all qubits involved in state preparation. Following points are discuss the detailed contributions of this study.

1. We undertake a detailed analysis of four standard quantum image encoding algorithms that represents various views in different way. Includes, FRQI method, QPIE method, OQIM method, and EFRQI method in detailed in both theoretical and practical implementation information.
2. Two situations are considered: One is noise-free simulation using pure quantum states as state vectors to demonstrate baseline behavior of the encoding algorithms performance, and Secondly noisy simulation where BF, PF, AD, PD, and DN noise channels are applied to all qubits in the encoding circuit part, these are simulated using mixed quantum states to analyse the impact of different type of noises.
3. We assess the results of both noise and noise-free reconstructed output images using standard common metrics, such as MSE, PSNR in dB, SSIM, and IoU, to obtain a comprehensive understanding of the effects of quantum noise channels. This metric would measure the impact of noise that how it can be reduce the various property of the input image information's.

3 Background

3.1 Quantum Image Representation

In this paper, four types of quantum image encoding algorithms were examined and implemented: FRQI [6], QPIE [14], OQIM [13], and EFRQI [8]. An overview of the circuit architecture procedure of the selected quantum image encoding algorithms, including their corresponding classical preprocessing details, is illustrated in Figure 1.

3.1.1 Flexible Representation of Quantum Images (FRQI)

In 2011, Le et al. proposed a quantum image encoding algorithm called Flexible Representation of Quantum Images (FRQI) [6]. This representation encodes grayscale images as normalized quantum states, capturing both color information and corresponding pixel positions. FRQI provides a foundation for polynomial preparation, image compression, and various quantum image processing operations. The working process of FRQI is presented in Figure 1. For representing a $2^n \times 2^n$ image, this method requires two registers:

A position qubit register that uses $2n$ qubits and a color qubit register that uses 1 qubit to encode the classical image as quantum information. In FRQI, the required classical preprocessing step converts each grayscale intensity value $I \in [0, 255]$ into a corresponding rotation angle using the mapping $\theta = \frac{I}{255} \times \frac{\pi}{2}$.

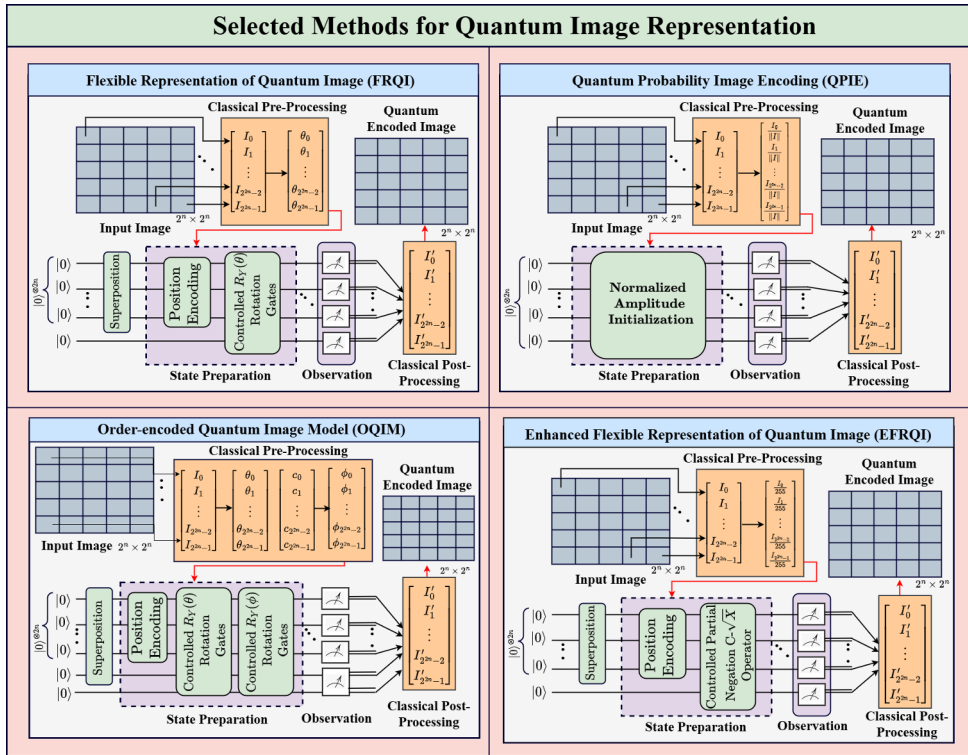


Figure 1. Overview of the architecture of selected quantum image encoding algorithms, including their corresponding classical pre-processing specifications.

Implementation of FRQI:

First, initialize the $2n + 1$ qubits as $|0\rangle^{\otimes(2n+1)}$

$$|\psi_0\rangle = |0\rangle \otimes |0\rangle^{\otimes 2n} \tag{1}$$

Then, apply a Hadamard gate to the position $2n$ qubits, which results in:

$$|\psi_1\rangle = \frac{1}{\sqrt{2^n}} \sum_{i=0}^{2^{2n}-1} |0\rangle \otimes |i\rangle \tag{2}$$

Next, controlled rotations are applied successively corresponding to each spatial pixel position as:

$$|\text{img}(\theta)\rangle = \prod_{i=0}^{2^{2n}-1} R_i |\psi_1\rangle = R_{2^{2n}-1} (R_{2^{2n}-2} (\dots (R_1 (R_0 |\psi_1\rangle)))) \tag{3}$$

where R_i is the controlled rotation operation defined as:

$$R_i = \left(I \otimes \sum_{\substack{j=0 \\ j \neq i}}^{2^{2n}-1} |j\rangle \langle j| \right) + (R_y(2\theta_i) \otimes |i\rangle \langle i|) \tag{4}$$

The rotation gate $R_y(2\theta_i)$ is given by: $R_y(2\theta_i) = \begin{bmatrix} \cos \theta_i & -\sin \theta_i \\ \sin \theta_i & \cos \theta_i \end{bmatrix}$. In Equation 4, the rotation gate applied to the color qubit when the position qubits are in state $|i\rangle$; otherwise, the identity operation is applied to the remaining pixel positions.

When expanding the first term $R_0|\psi_1\rangle$, we get:

$$R_0|\psi_1\rangle = \left[\left(I \otimes \sum_{\substack{j=1 \\ j \neq 0}}^{2^{2n}-1} |j\rangle\langle j| \right) + (R_y(2\theta_0) \otimes |0\rangle\langle 0|) \right] \left(\frac{1}{2^n} \sum_{i=0}^{2^{2n}-1} |0\rangle \otimes |i\rangle \right) \quad (5)$$

$$= \frac{1}{2^n} \left[\left(|0\rangle \otimes \sum_{j=1}^{2^{2n}-1} |j\rangle \right) + (\cos(\theta_0)|0\rangle + \sin(\theta_0)|1\rangle) \otimes |0\rangle \right] \quad (6)$$

By applying all rotations successively as in Equation 3, we obtain:

$$\begin{aligned} |\psi(\theta)\rangle = \frac{1}{2^n} & \left[(\cos(\theta_0)|0\rangle + \sin(\theta_0)|1\rangle) \otimes |0\rangle \right. \\ & + (\cos(\theta_1)|0\rangle + \sin(\theta_1)|1\rangle) \otimes |1\rangle \\ & + \dots \\ & \left. + (\cos(\theta_{2^{2n}-1})|0\rangle + \sin(\theta_{2^{2n}-1})|1\rangle) \otimes |2^{2n}-1\rangle \right] \quad (7) \end{aligned}$$

From this state, we obtain the final FRQI representation:

$$|\psi(\theta)\rangle = \frac{1}{2^n} \sum_{i=0}^{2^{2n}-1} (\cos(\theta_i)|0\rangle + \sin(\theta_i)|1\rangle) \otimes |i\rangle \quad (8)$$

where θ_i belongs to the closed interval of $0, \pi/2$, for $i = 0, 1, \dots, 2^{2n}-1$. Here, the classical intensity values are encoded as rotation angles through the color qubit. After the circuit implementation, the pixel intensity information is encoded in the rotation angles as described in Equation 8. To retrieve the classical image, all $2n+1$ qubits are measured. For each pixel position $|i\rangle$, the corresponding classical intensity value is reconstructed from the measurement probabilities of the color qubit.

Let $P(0, i)$ and $P(1, i)$ denote the joint probabilities of observing the color qubit in states $|0\rangle$ and $|1\rangle$, respectively, while the position register collapses to $|i\rangle$. The normalized conditional probabilities are expressed as: $P_0(i) = \frac{P(0,i)}{P(0,i)+P(1,i)}$, $P_1(i) = \frac{P(1,i)}{P(0,i)+P(1,i)}$.

The classical intensity at the i -th position, I'_i , can be reconstructed from either the probability of measuring $|0\rangle$ or $|1\rangle$ on the color qubit when the position register collapses to $|i\rangle$. That is:

$$I'_i = \begin{cases} \frac{255}{\pi/2} \arccos(\sqrt{P_0(i)}), & \text{if the color qubit is measured in } |0\rangle, \\ \frac{255}{\pi/2} \arcsin(\sqrt{P_1(i)}), & \text{if the color qubit is measured in } |1\rangle. \end{cases} \quad (9)$$

Both expressions yield the same reconstructed intensity. Thus, the classical grayscale value can be consistently recovered from the quantum measurement statistics.

3.1.2 Quantum Probability Image Encoding (QPIE)

In 2017, Yao et al. proposed QPIE encoding method [14], which distinguishes itself from alternative encoding methods through its computational efficiency, particularly in qubit utilization. For a classical image of size $r \times c$, QPIE requires only $\lceil \log_2(rc) \rceil$ qubits to represent it in a quantum circuit, where r is the number of rows and c denotes the number of columns. The detailed working procedure of this representation is shown in Figure 1.

For a general size $2^n \times 2^n$ image is represented as a quantum image using QPIE encoding as follows:

$$|Img\rangle = \sum_{i=0}^{2^N-1} C_i |i\rangle, \quad \text{where } N = \lceil \log_2(rc) \rceil \quad (10)$$

Here C_i represents the Normalized classical pixel intensity, and $|i\rangle$ corresponds to the quantum state associated with the pixel position in the image its range from $i = 0, 1, 2, \dots, 2^N - 1$. To ensure that the coefficients in Equation 10 preserve the normalization condition of quantum superposition, each coefficient C_i is computed as:

$$C_i = \frac{I_i}{\|I\|} = \frac{I_i}{\sqrt{\sum_{i=0}^{2^N-1} I_i^2}}, \quad \text{if } \|I\| > 0$$

where I_i represents the classical intensity value at pixel position i . This normalization ensures that the quantum state remains valid, satisfying the condition $\sum_{i=0}^{2^N-1} |C_i|^2 = 1$. Expanding Equation 10, the quantum image state can be expressed as:

$$|Img\rangle = C_0|0\rangle + C_1|1\rangle + \dots + C_{2^N-2}|2^N - 2\rangle + C_{2^N-1}|2^N - 1\rangle \quad (11)$$

Thus, the state vector representation of $|Img\rangle$ is given by: $\begin{bmatrix} C_0 \\ C_1 \\ C_2 \\ \vdots \\ C_{2^N-1} \end{bmatrix}$ which is an $(2^N \times 1)$

column vector representing the quantum state of the image. Now, each pixel position $|i\rangle$ has an amplitude that represents the pixel intensity in normalized way, to ensure that the quantum state satisfies the normalization requirements. After the quantum circuit execution, the classical image is reconstructed through measurement. The probability of observing basis state $|i\rangle$, denoted as Probability_i , corresponds to the squared amplitude $|C_i|^2$. Thus, the reconstructed classical intensity at pixel position i is obtained as:

$$I'_i = \sqrt{\text{Probability}_i} \|I\| \quad (12)$$

3.1.3 Order-encoded Quantum Image Model (OQIM)

In 2019, Guanlei Xu et al. proposed the OQIM encoding method [13]. Unlike conventional quantum image representation methods that only store gray intensity information, OQIM also encodes the sorted order of pixel information during the image preparation stage itself. This additional encoding enables histogram specification for the multiple images simultaneously, significantly improving the efficiency of histogram equalization and related image enhancement tasks in the quantum domain. The detailed working procedure of this method is illustrated in Figure 1. OQIM uses two quantum registers to represent a $2^n \times 2^n$ grayscale image:

A first 2-qubit register that stores both the grayscale intensity and the real coordinate information of each pixel, and a second $2n$ -qubit register that stores the sorted pixel positions through Hadamard superposition states. The OQIM representation of a quantum image is defined as:

$$|\text{Image}\rangle = \frac{1}{2^{n+\frac{1}{2}}} \sum_{i=0}^{2^n-1} |cp_i\rangle \otimes |i\rangle \quad (13)$$

where the first register $|cp_i\rangle$ encodes both color and actual coordinate information through the basis states $\{|00\rangle, |01\rangle, |10\rangle, |11\rangle\}$ as: $|cp_i\rangle = \cos(\theta_i)|00\rangle + \sin(\theta_i)|10\rangle + \cos(\phi_i)|01\rangle + \sin(\phi_i)|11\rangle$ and $|i\rangle$ represents the sorted position encoded in the basis states of a $2n$ -qubit sequence. Before quantum encoding, classical preprocessing is required to map pixel information to rotation angles: The grayscale intensity values I_i are mapped to rotation angles θ_i through: $\theta_i = \frac{I_i}{255} \times \frac{\pi}{2}$, $\theta_i \in [0, \frac{\pi}{2}]$ where $\theta = (\theta_0, \theta_1, \dots, \theta_{2^n-1})$ represents all intensity angles. The real coordinate pixel positions $c_i \in \{0, 1, 2, \dots, 2^{2n} - 1\}$ are mapped to rotation angles ϕ_i through: $\phi_i = \frac{c_i}{N-1} \times \frac{\pi}{2}$, $\phi_i \in [0, \frac{\pi}{2}]$ where $\phi = (\phi_0, \phi_1, \dots, \phi_{2^n-1})$ and $N = 2^{2n}$ is the total pixels count in the image. Here the intensity angles satisfy $\theta_i \leq \theta_j$ if $i < j$ for $i, j \in \{0, 1, \dots, 2^{2n} - 1\}$, meaning the values are encoded in ascending order based on gray intensity.

The normalization condition verifies that OQIM represents a valid quantum state:

$$\| |\text{Image}\rangle \| = \frac{1}{2^{n+\frac{1}{2}}} \sqrt{\sum_{i=0}^{2^n-1} (\cos^2 \theta_i + \sin^2 \theta_i + \cos^2 \phi_i + \sin^2 \phi_i)} = 1 \quad (14)$$

Implementation of OQIM:

The quantum circuit implementation of OQIM consists of the following steps: Initialize $2n+2$ qubits in the $|0\rangle$ state:

$$|\psi_0\rangle = |0\rangle^{\otimes(2+2n)} = |0\rangle_c \otimes |0\rangle_p \otimes |0\rangle^{\otimes 2n} \quad (15)$$

where $|0\rangle_c$ is the color qubit, $|0\rangle_p$ is the real position qubit, and $|0\rangle^{\otimes 2n}$ represents the $2n$ index qubits. Apply Hadamard gates on $2n + 1$ qubits (excluding the color qubit) to create a superposition state:

$$|\psi_1\rangle = \frac{1}{2^{n+\frac{1}{2}}} |0\rangle_c \otimes (|0\rangle + |1\rangle)_p \otimes \sum_{i=0}^{2^n-1} |i\rangle \quad (16)$$

Define the rotation operators for encoding grayscale intensity and real coordinates:

$$R_y(2\theta) = \begin{bmatrix} \cos \theta & -\sin \theta \\ \sin \theta & \cos \theta \end{bmatrix}, \text{ and}$$

$R_y(2\phi) = \begin{bmatrix} \cos \phi & -\sin \phi \\ \sin \phi & \cos \phi \end{bmatrix}$. The controlled rotation matrices are defined as: *For color qubit rotation:* $R_{c,i} = R_y(2\theta_i) \otimes |0\rangle\langle 0|_p$ applies $R_y(2\theta_i)$ on the color qubit when the position qubit is $|0\rangle$, and *For position qubit rotation:* $R_{p,i} = R_y(2\phi_i) \otimes |1\rangle\langle 1|_p$ applies $R_y(2\phi_i)$ on the color qubit when the position qubit is $|1\rangle$.

The combined rotation operator for the i -th position is: $R_i = R_{c,i} \cdot R_{p,i}$

The controlled rotation operator conditioned on the index register being in state $|i\rangle$ is:

$$R_{c,p,i} = \left(I^{\otimes 2} \otimes \sum_{\substack{j=0 \\ j \neq i}}^{2^n-1} |j\rangle\langle j| \right) + (R_i \otimes |i\rangle\langle i|) \quad (17)$$

Apply the controlled rotation operators sequentially to all positions: $R_{cp} = \prod_{j=0}^{2^{2n}-1} R_{cp,j}$ and applying R_{cp} to the state $|\psi_1\rangle$ yields the final OQIM state:

$$|\text{Image}\rangle = \frac{1}{2^{n+\frac{1}{2}}} \sum_{i=0}^{2^{2n}-1} \left(\cos(\theta_i) |00\rangle + \sin(\theta_i) |10\rangle + \cos(\phi_i) |01\rangle + \sin(\phi_i) |11\rangle \right) \otimes |i\rangle \quad (18)$$

To retrieve the classical image from the OQIM circuit, all $2n + 2$ qubits are measured. The classical intensity at the i -th sorted position can be reconstructed using the conditional probabilities $P_{10}(i)$ and $P_{11}(i)$ for the corresponding basis states, where:

$$P_{10}(i) = \frac{P(|10\rangle, |i\rangle)}{P(i)}, \quad P_{11}(i) = \frac{P(|11\rangle, |i\rangle)}{P(i)} \quad (19)$$

The rotation angles are then recovered as: $\theta_i = \arcsin(\sqrt{2 \cdot P_{10}(i)})$, $\phi_i = \arcsin(\sqrt{2 \cdot P_{11}(i)})$ and the grayscale intensity and real coordinate position are then recovered as: $I'_i = \theta_i \times \frac{255 \times 2}{\pi}$, $c'_i = \phi_i \times \frac{(N-1) \times 2}{\pi}$ where $N = 2^{2n}$ is the total number of pixels in the image.

3.1.4 Enhanced Flexible Representation of Quantum Images (EFRQI)

In 2021, Nasr *et al.* proposed an improved version of FRQI known as the Enhanced Flexible Representation of Quantum Images (EFRQI) [8]. Similar to FRQI, this approach uses two quantum registers to represent a $2^n \times 2^n$ grayscale image: a position register consisting of $2n$ qubits and a single color qubit, resulting in a total requirement of $2n + 1$ qubits. The key modifications that are made to EFRQI include: the utilization of the *Partial Negation Operator*[15] that enables the use of an alternative and efficient process of encoding the grayscale intensity values to the quantum state.

The k -th root of the Pauli-X gate is used to define the Partial Negation Operator. The operator RX_k is given as:

$$RX_k = \sqrt[k]{X} = \frac{1}{2} \begin{bmatrix} 1 + \sqrt[k]{-1} & 1 - \sqrt[k]{-1} \\ 1 - \sqrt[k]{-1} & 1 + \sqrt[k]{-1} \end{bmatrix}.$$

When applied to the computational basis states, its action is:

$$RX_k|0\rangle = \frac{1 + \sqrt[k]{-1}}{2}|0\rangle + \frac{1 - \sqrt[k]{-1}}{2}|1\rangle,$$

$$RX_k|1\rangle = \frac{1 - \sqrt[k]{-1}}{2}|0\rangle + \frac{1 + \sqrt[k]{-1}}{2}|1\rangle.$$

Applying the operator I times yields:

$$RX_k^I = \frac{1}{2} \begin{bmatrix} 1 + (-1)^{I/k} & 1 - (-1)^{I/k} \\ 1 - (-1)^{I/k} & 1 + (-1)^{I/k} \end{bmatrix}.$$

When the case of $I = k$ the operator is standard Pauli-X gate: $(RX_k)^k = X$. Application of EFRQI in the context of image encoding, this property is used by fixing $k = 255$ (represents the full range of grayscale intensity levels) when using the common 8-bit grayscale images, where the pixel intensities $I = [0, 255]$. The intensity of each pixel, denoted as I is used to encode the grayscale information by using the partial negation operator which is applied by the number of times.

Implementation of EFRQI:

To construct the EFRQI representation, first prepares a total of $2n + 1$ qubits, one color qubit, and $2n$ position qubits.

$$|\psi_0\rangle = |0\rangle \otimes \underbrace{|0\rangle \otimes |0\rangle \otimes \cdots \otimes |0\rangle}_{2n \text{ qubits}}. \quad (20)$$

Then, a Hadamard gate is applied on all $2n$ position qubits:

$$|\psi_1\rangle = \frac{1}{2^n} \sum_{i=0}^{2^{2n}-1} |0\rangle \otimes |i\rangle. \quad (21)$$

After preparing the superposition state, the grayscale intensity values are encoded using the Partial Negation Operator. For each pixel position i , the operator $RX_k^{I_i}$ is applied to the color qubit, where I_i denotes the classical grayscale intensity of the pixel and $k = 255$ corresponds to the full intensity range:

$$|\psi_2\rangle = \frac{1}{2^n} \sum_{i=0}^{2^{2n}-1} RX_k^{I_i} |0\rangle \otimes |i\rangle. \quad (22)$$

Using the definition of the repeated partial negation operator, the color qubit transforms as:

$$RX_k^{I_i} |0\rangle = \frac{1 + (-1)^{I_i/k}}{2} |0\rangle + \frac{1 - (-1)^{I_i/k}}{2} |1\rangle.$$

Substituting this expansion into the quantum image state gives:

$$|\psi_2\rangle = \frac{1}{2^n} \sum_{i=0}^{2^{2n}-1} \left[\frac{1 + (-1)^{I_i/k}}{2} |0\rangle + \frac{1 - (-1)^{I_i/k}}{2} |1\rangle \right] \otimes |i\rangle. \quad (23)$$

Thus, in EFRQI, each grayscale intensity value I_i is embedded into the quantum image through the exponent of the Partial Negation Operator, providing a flexible and efficient encoding scheme.

After the circuit implementation, the classical intensity value I'_i is reconstructed from the quantum measurement outcomes in the same manner as in the FRQI scheme, as described in Equation 9.

3.2 Quantum Noise and Error Channels

Quantum computing represents a crucial advancement in modern technology. However, devices operating in the current NISQ era are significantly affected by various sources of noise and operational errors [10], which limit the reliability and scalability of quantum algorithms. To analyze how noise affects quantum states, we use the density-matrix representation ρ , which is suitable for both pure and mixed states. For a single qubit, the Idle density matrix is written as

$$\rho = \begin{bmatrix} \rho_{00} & \rho_{01} \\ \rho_{10} & \rho_{11} \end{bmatrix},$$

where ρ_{00} and ρ_{11} denote the populations of the $|0\rangle$ and $|1\rangle$ states, and the off-diagonal elements ρ_{01} and ρ_{10} represent the coherence between these basis states. The evolution of a quantum system under noise is described using a quantum operation \mathcal{E} , which models how noise processes modify a density matrix [9]. If ρ is the initial state and ρ' is the noisy state, the

Table 1. Comparison of different quantum noise channels and their characteristics on a single-qubit quantum system.

Channel	Properties
Bit Flip Noise	Nature: Flips computational basis states
	Kraus Operators: $K_0 = (\sqrt{1-p}) \cdot I$, $K_1 = (\sqrt{p}) \cdot X$
	Evolved Density Matrix ρ': $\begin{bmatrix} (1-p)\rho_{00} + p\rho_{11} & (1-p)\rho_{01} + p\rho_{10} \\ (1-p)\rho_{10} + p\rho_{01} & (1-p)\rho_{11} + p\rho_{00} \end{bmatrix}$
	Impact: $ 0\rangle \leftrightarrow 1\rangle$ exchange
	PennyLane Syntax: BitFlip(p, wires=i)
Phase Flip Noise	Nature: Flips relative phase
	Kraus Operators: $K_0 = (\sqrt{1-p}) \cdot I$, $K_1 = (\sqrt{p}) \cdot Z$
	Evolved Density Matrix ρ': $\begin{bmatrix} \rho_{00} & (1-2p)\rho_{01} \\ (1-2p)\rho_{10} & \rho_{11} \end{bmatrix}$
	Impact: Phase coherence loss; off-diagonal elements decay
	PennyLane Syntax: PhaseFlip(p, wires=i)
Amplitude Damping Noise	Nature: Energy dissipation to environment
	Kraus Operators: $K_0 = \begin{pmatrix} 1 & 0 \\ 0 & \sqrt{1-\gamma} \end{pmatrix}$, $K_1 = \begin{pmatrix} 0 & \sqrt{\gamma} \\ 0 & 0 \end{pmatrix}$
	Evolved Density Matrix ρ': $\begin{bmatrix} \rho_{00} + \gamma\rho_{11} & \sqrt{1-\gamma}\rho_{01} \\ \sqrt{1-\gamma}\rho_{10} & (1-\gamma)\rho_{11} \end{bmatrix}$
	Impact: $ 1\rangle \rightarrow 0\rangle$ decay; population loss
	PennyLane Syntax: AmplitudeDamping(gamma, wires=i)
Phase Damping Noise	Nature: Loss of quantum coherence
	Kraus Operators: $K_0 = \begin{pmatrix} 1 & 0 \\ 0 & \sqrt{1-\gamma} \end{pmatrix}$, $K_1 = \begin{pmatrix} 0 & 0 \\ 0 & \sqrt{\gamma} \end{pmatrix}$
	Evolved Density Matrix ρ': $\begin{bmatrix} \rho_{00} & \sqrt{(1-\gamma)}\rho_{01} \\ \sqrt{(1-\gamma)}\rho_{10} & \rho_{11} \end{bmatrix}$
	Impact: Off-diagonal terms decay; populations unchanged
	PennyLane Syntax: PhaseDamping(gamma, wires=i)
Depolarizing Noise	Nature: Random Pauli errors
	Kraus Operators: $K_0 = (\sqrt{1-p}) \cdot I$, $K_1 = (\sqrt{p/3}) \cdot X$, $K_2 = (\sqrt{p/3}) \cdot Y$, and $K_3 = (\sqrt{p/3}) \cdot Z$
	Evolved Density Matrix ρ': $\begin{bmatrix} (1-\frac{2p}{3})\rho_{00} + \frac{2p}{3}\rho_{11} & (1-\frac{4p}{3})\rho_{01} \\ (1-\frac{4p}{3})\rho_{10} & (1-\frac{2p}{3})\rho_{11} + \frac{2p}{3}\rho_{00} \end{bmatrix}$
	Impact: Complete randomization toward maximally mixed state
	PennyLane Syntax: DepolarizingChannel(p, wires=i)

action of a quantum noise channel is expressed as $\rho' = \varepsilon(\rho)$. Such channels are typically represented using Kraus operators $\{K_i\}$, which satisfy the completeness condition $\sum_i K_i^\dagger K_i = I$. In this form, the noisy evolution of the system is given by,

$$\varepsilon(\rho) = \sum_i K_i \rho K_i^\dagger \quad (24)$$

The Kraus operators used in quantum noise channels in Equation (24) are commonly constructed from the standard Pauli matrices. These matrices include the Identity operator I and the Pauli operators X , Y , and Z , defined as

$$I = \begin{bmatrix} 1 & 0 \\ 0 & 1 \end{bmatrix}, \quad X = \begin{bmatrix} 0 & 1 \\ 1 & 0 \end{bmatrix}, \quad Y = \begin{bmatrix} 0 & -i \\ i & 0 \end{bmatrix}, \quad Z = \begin{bmatrix} 1 & 0 \\ 0 & -1 \end{bmatrix}$$

Five main principal categories of quantum noise channels are studied in this paper: BF, PF, AD, PD, and DN noise channels. Each of these channels corresponds to a distinct physical error mechanism that affects the stability and fidelity of quantum information.

3.2.1 Bit Flip (p)

The Bit-Flip (BF) channel models the error in which a qubit is flipped from $|0\rangle$ to $|1\rangle$ or vice versa, similar to applying a Pauli- X gate. With probability $p \in [0, 1]$, the qubit undergoes this flip, and with probability $1 - p$, it remains unchanged. The channel is described by the following single-qubit Kraus operators in Equation 25:

$$K_0 = \sqrt{1-p} \begin{bmatrix} 1 & 0 \\ 0 & 1 \end{bmatrix}, \quad K_1 = \sqrt{p} \begin{bmatrix} 0 & 1 \\ 1 & 0 \end{bmatrix}, \quad (25)$$

3.2.2 Phase Flip (p)

The Phase-Flip (PF) channel models an error in which only the phase of a qubit is altered while its probability amplitudes remain unchanged. This is symbolized by the Pauli- Z gate that leaves the state of $|0\rangle$ unchanged and multiplies the state of $|1\rangle$ by -1 , the equivalent of a phase shift of π . The noise process has a probability of happening depending on a probability parameter $p \in [0, 1]$, whereby the noise is modeled by the following Kraus operators:

$$K_0 = \sqrt{1-p} \begin{bmatrix} 1 & 0 \\ 0 & 1 \end{bmatrix}, \quad K_1 = \sqrt{p} \begin{bmatrix} 1 & 0 \\ 0 & -1 \end{bmatrix}, \quad (26)$$

3.2.3 Amplitude Damping (γ)

Amplitude damping (AD) is a model that follows the dissipation of energy in the qubit, in which the excited state of the qubit $|1\rangle$, decays to the ground state $|0\rangle$. That noise has a damping probability which is denoted as γ ranging from 0 to 1. The channel is described by the following single-qubit Kraus operators in Equation 27:

$$K_0 = \begin{bmatrix} 1 & 0 \\ 0 & \sqrt{1-\gamma} \end{bmatrix}, \quad K_1 = \begin{bmatrix} 0 & \sqrt{\gamma} \\ 0 & 0 \end{bmatrix}, \quad (27)$$

3.2.4 Phase Damping (γ)

Phase damping (PD), also known as phase relaxation or dephasing, is a quantum noise process that causes a loss of phase coherence without altering the population of the energy levels. Unlike amplitude damping, which changes the qubit state, phase damping only reduces the off-diagonal elements of the density matrix, representing the gradual decay of quantum superposition. The process occurs with damping probability $\gamma \in [0, 1]$.

This channel is described by the following single-qubit Kraus operators in Equation 28:

$$K_0 = \begin{bmatrix} 1 & 0 \\ 0 & \sqrt{1-\gamma} \end{bmatrix}, \quad K_1 = \begin{bmatrix} 0 & 0 \\ 0 & \sqrt{\gamma} \end{bmatrix}, \quad (28)$$

3.2.5 Depolarization Channel (p)

The depolarization channel (DN) is a fundamental noise model that describes a situation where a qubit loses its quantum information to the environment in a completely basis-independent manner. Unlike specific error models such as bit-flip or phase-flip channels that affect only particular components of a qubit's state, depolarizing noise acts uniformly in all directions on the Bloch sphere. When a depolarizing error occurs, the qubit is replaced by a maximally mixed state with probability p , thereby erasing coherence and reducing the purity of the quantum state. Mathematically, the corresponding channel for this DN is represented using the Kraus operators in Equation 29, where the depolarization probability $p \in [0, 1]$ is evenly distributed across the Pauli operations. The Kraus operators are defined as:

$$\begin{aligned} K_0 &= \sqrt{1-p} \begin{bmatrix} 1 & 0 \\ 0 & 1 \end{bmatrix}, & K_1 &= \sqrt{\frac{p}{3}} \begin{bmatrix} 0 & 1 \\ 1 & 0 \end{bmatrix}, \\ K_2 &= \sqrt{\frac{p}{3}} \begin{bmatrix} 0 & -i \\ i & 0 \end{bmatrix}, & K_3 &= \sqrt{\frac{p}{3}} \begin{bmatrix} 1 & 0 \\ 0 & -1 \end{bmatrix}. \end{aligned} \quad (29)$$

A comprehensive overview of the characteristics of quantum noise channels and their respective impacts on quantum state evolution is presented in Table 1.

4 Methodology

This paper examines four methods of quantum image encoding to determine how the circuit design affects the performance of image representation in both ideal noise free and noisy conditions. The most effective encoding models are then analyzed in the perspective of realistic quantum device noise to determine their coherence and relevance in the actual world when it comes to the applications in image processing. The methodology is based on three major steps that include the analysis of different parts of quantum image representation, encoding images in either a noisy or a noise-free environment, and measuring their effectiveness. The summary of the selected methodology is in Figure 2.

4.1 Different Aspects of Quantum Image Representation

This section discusses different perspectives on quantum image information storage by considering four representative quantum image encoding methods: FRQI [6], QPIE [14], OQIM [13], and EFRQI [8]. The detailed working procedures of these four methods are described in the previous section. These methods are selected because they differ significantly in terms of

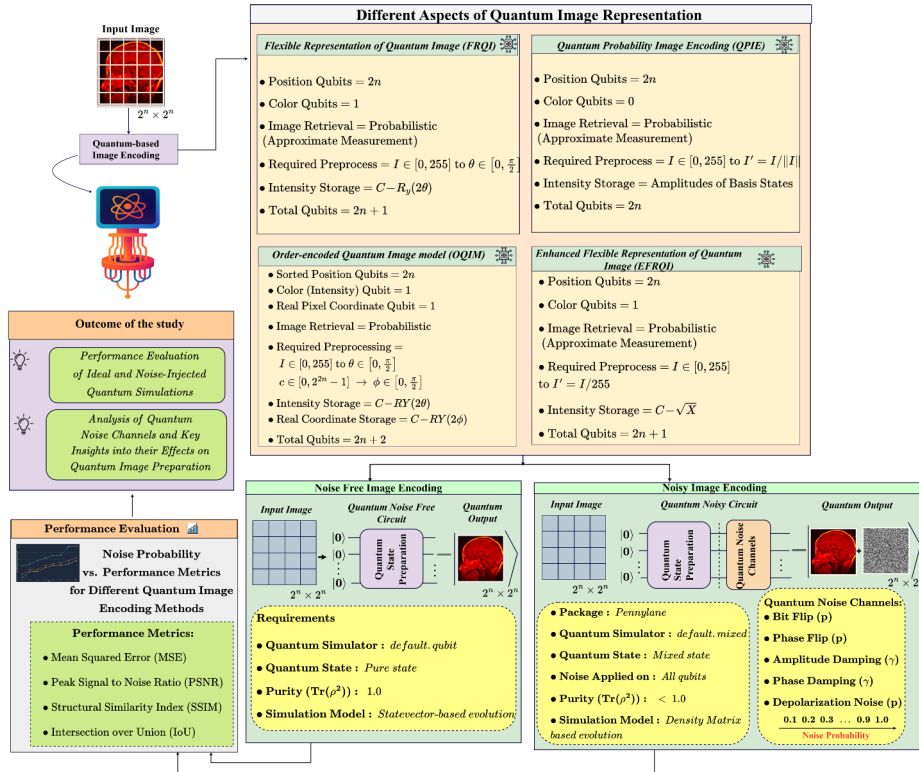


Figure 2. Comprehensive comparison of multiple quantum image representation perspectives evaluated under noise-free and quantum noise-affected conditions using the PennyLane simulator.

unitary gate construction, number of qubits required, classical preprocessing strategies, quantum state preparation mechanisms, and image retrieval through classical post-processing. Such variations enable a comprehensive examination of how image information can be stored and manipulated within quantum circuits from multiple architectural viewpoints. Accordingly, circuits based on these four representations are implemented and analyzed in the subsequent sections to evaluate their performance under different conditions.

4.2 Image Encoding

After constructing the required quantum image representation circuits, two encoding scenarios are considered. In the first scenario, noise-free image encoding is performed using an ideal quantum simulator without introducing any external quantum noise channels. Specifically, the PennyLane `default.qubit` simulator is employed to evaluate the intrinsic behavior of each encoding scheme and to obtain image reconstruction results that closely match the original classical image. This noise-free analysis serves as a baseline for assessing the ideal performance of the quantum image encoding circuits.

In the second scenario, noisy image encoding is carried out by introducing quantum noise channels on all qubits after state preparation using the PennyLane `default.mixed` simulator. The quantum noise models considered are described in the previous sections. By decoding the circuit outputs obtained under noisy conditions, this analysis enables a systematic evaluation

of how different noise sources affect quantum state preparation and image reconstruction quality. The comparative analysis between noise-free and noisy encoding provides insights into the robustness and practical feasibility of the proposed quantum image representation methods.

4.3 Performance Evaluation

To quantitatively evaluate the performance of different quantum image encoding algorithms under noise-free and noisy simulation environments, four widely used image quality metrics are considered. These evaluation metrics are commonly employed for assessing image reconstruction and edge preservation performance, and their detailed descriptions can be found in [11]. The metrics used in this study are summarized as follows.

(i) Mean Squared Error (MSE): MSE measures the average squared difference between the quantum reconstructed image and the ground-truth classical image. It is defined as

$$\text{MSE} = \frac{1}{128 \times 128} \sum_{i=0}^{127} \sum_{j=0}^{127} [P(i, j) - G(i, j)]^2 \quad (30)$$

where $P(i, j)$ denotes the reconstructed quantum image and $G(i, j)$ represents the ground-truth classical image.

(ii) Peak Signal-to-Noise Ratio (PSNR): PSNR quantifies the reconstruction quality by relating the maximum possible pixel intensity to the corresponding MSE value. It is expressed in decibels (dB) as

$$\text{PSNR} = 10 \log_{10} \left(\frac{1}{\text{MSE}} \right) \quad (31)$$

A higher PSNR value indicates better reconstruction fidelity.

(iii) Structural Similarity Index Measure (SSIM):

The SSIM is a perceptual metric used to calculate the similarity in two images based on luminance, contrast, and structure. The formula for the SSIM calculation for the reconstructed image P and the actual image G is given

$$\text{SSIM}(P, G) = l(P, G) \cdot c(P, G) \cdot s(P, G) \quad (32)$$

where $l(P, G)$, $c(P, G)$, and $s(P, G)$ represent luminance, contrast, and structural comparisons, respectively.

(iv) Intersection over Union (IoU):

IoU quantifies how well the reconstructed image P matches the ground-truth image G . It is defined as

$$\text{IoU} = \frac{|P \cap G|}{|P \cup G|} \quad (33)$$

Where $|P \cap G|$ is the number of pixels totally match in both images P and G , and $|P \cup G|$ is the total number of pixels in either image. These defined metrics collectively provide a complete evaluation of the performance of different quantum image encoding algorithms in the case of with noise and without noise simulation environments.

5 Experimental Results

In this section, the selected quantum image encoding algorithms are implemented using the Python-based PennyLane framework. A 64×64 grayscale image selected from the Kaggle dataset is used as the input.

Figure 4 presents the obtained results for FRQI, QPIE, OQIM, and EFRQI using an ideal noise-free simulator. Although all the selected encoding methods are originally designed for grayscale images, a classical ‘hot colormap’ is applied to the reconstructed quantum images for improved visual interpretation.

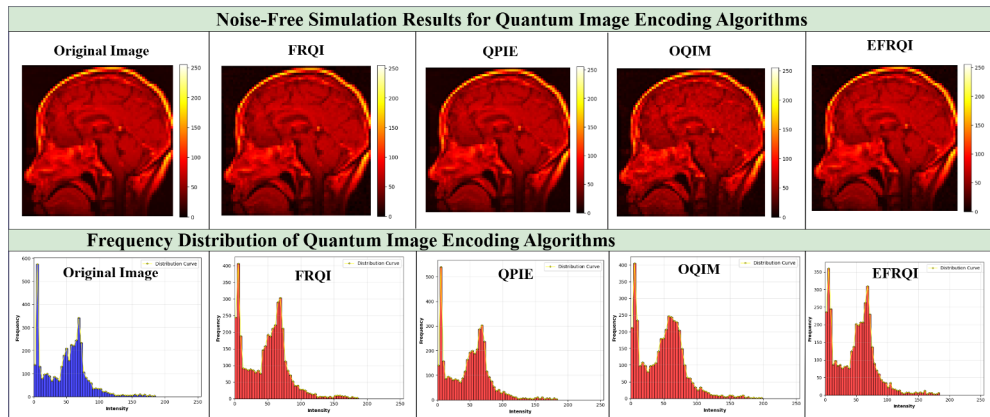


Figure 4. Implementation of four different quantum image encoding algorithms with their corresponding intensity distributions under a noise-free simulator.

In addition, this figure includes the corresponding intensity (frequency) distributions for each encoding method. From the frequency distribution analysis, the QPIE encoding exhibits a distribution that is closest to the actual intensity distribution of the original image. The remaining three encoding methods, while showing minor deviations in distribution, effectively preserve the overall visual characteristics of the classical image.

Figure 5 illustrates the quantitative evaluation of the quantum image encoding algorithms in terms of MSE, PSNR, SSIM, and IoU for different shot sizes under an ideal (noise-free) simulation using the `default.qubit` simulator. The findings show that the number of measurements within the range of 9.1×10^6 to 9.8×10^6 exhibit consistent repetition behavior. As the shot size increases, the MSE continuously decreases for all four encoding methods, while PSNR, SSIM, and IoU show monotonic increases. The figure confirms that when increasing the number of shots during the circuit execution impacts the output reconstructed image as closer to the original images. Among these four selected encoding methods, QPIE has low MSE metric and higher PSNR, SSIM, IOU values. QPIE converges quickly to the minimum MSE value compared to remaining encoding. Which indicates the QPIE’s superior image fidelity compared to others. Figure 6 presents the circuit results of the selected encoding methods under five different quantum noise types, with probability of noise implemented as minimum 1% to maximum 100% to observe the effect in the two extremes.

Under the bit-flip noise channel, the QPIE method exhibits partial image collapse at $p = 0.1$, while a complete bit-wise inversion of the original image is observed at $p = 1$.

Similar collapse patterns are observed for FRQI and EFRQI under increasing bit-flip probability. In contrast, OQIM demonstrates more severe degradation even at lower noise

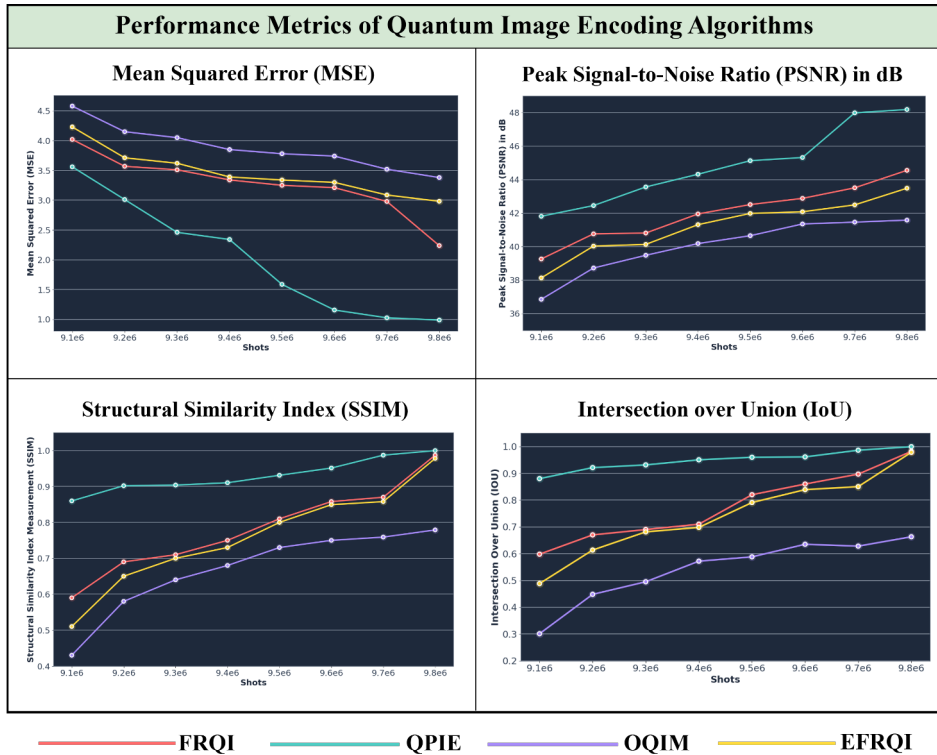


Figure 5. Quantitative results of quantum image encoding algorithms for different shot sizes under a noise-free simulator.

levels. For the phase-flip noise channel, no observable changes occur in the reconstructed images across all four encoding methods. This behavior is consistent with the property of phase-flip noise, which affects only the coherence terms by a factor of $(1 - 2p)$ while leaving the population states unchanged, as summarized in Table 1.

Under amplitude damping noise, distinct performance differences are observed among the encoding schemes. At $p = 0.1$, FRQI experiences minimal degradation, whereas QPIE shows noticeable information loss and OQIM exhibits the most severe degradation. EFRQI shows moderate information loss at this noise level. At $p = 1$, all encoding methods converge to an identical output, which is expected since amplitude damping causes complete decay of the $|1\rangle$ population to $|0\rangle$, resulting in a final state dominated by $|0\rangle$ population, in accordance with the noise characteristics listed in Table 1.

A similar trend to the phase-flip case is observed under phase-damping noise, where no visible variations or image collapse occur for any of the four encoding methods. This is attributed to the fact that phase-damping noise affects only the off-diagonal coherence terms and does not alter the population probabilities.

In the case of DN noise channel, significant degradation is observed due to random Pauli errors along the X , Y , or Z axes. For FRQI and EFRQI, substantial information loss occurs at $p = 0.1$, and complete image collapse is observed at $p = 1$. OQIM exhibits severe information loss even at lower noise levels, with almost no useful image information retained. QPIE demonstrates comparatively better robustness, showing limited degradation at $p = 0.1$, while

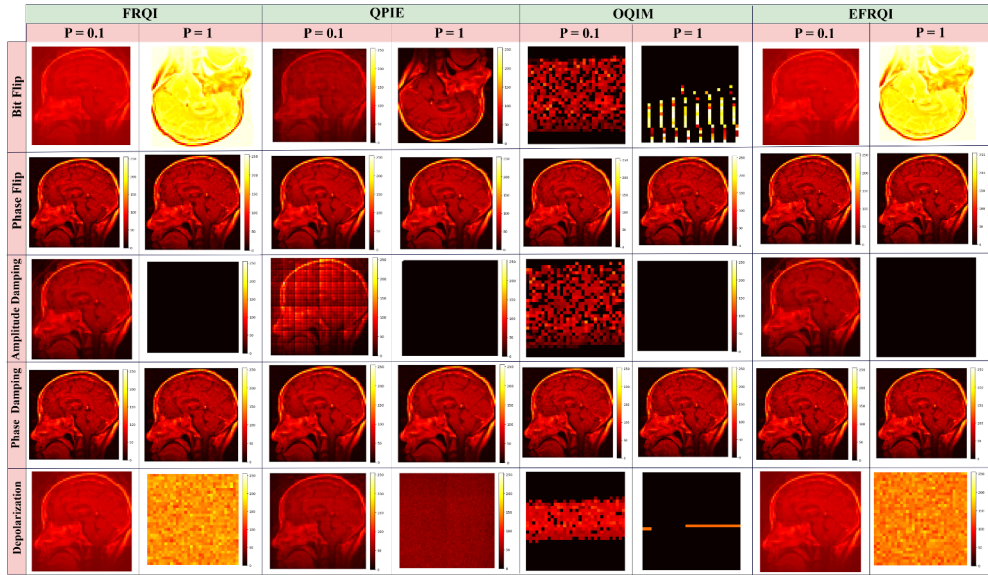


Figure 6. Implementation results of quantum image encoding algorithms examined under a noisy mixed state simulator using various noise probability values from 0.1 and 1.0 across five quantum noise channels.

at $p = 1$ the output corresponds to a randomly collapsed image. Overall, the results indicate that phase-flip and phase-damping noise channels do not significantly affect quantum image state preparation, as these channels do not alter population states. FRQI and EFRQI exhibit similar performance due to their closely related encoding structures, differing primarily in unitary operations.

OQIM exhibits the highest sensitive to the quantum noise, which can due to the following causes, its larger qubit requirement as $(2n+2)$ and the different way of classical preprocessing strategy, making this as more sensitive to noise accumulation during the circuit execution. Among the four selected quantum encoded algorithms, QPIE demonstrates better robustness comparatively against noise, owing to its lower number of qubit requirements $2n$ and minimal circuit depth complexity, resulting in fewer quantum gate operations while encoding.

The quantitative performance analysis of quantum image state preparation through five quantum noise channels is illustrated in Figure 7 based on MSE, PSNR, SSIM, and IoU. QPIE is better robust in the bit-flip noise channel out of all the three encoding methods in all measures. FRQI and EFRQI have almost the same performance, as they share similar encoding structures and circuit design, and OQIM suffers a great loss of information with the increase in the noise probability, which leads to the rise of MSE and the decrease of PSNR, SSIM, and IoU values.

In the case of the PF and PD noise channels, the value of defined performance measures is fairly similar with the different noise probability values of 0 to 1 in towards all four of the chosen encoding methods. It is this behavior that is in agreement with the theoretical properties of these noises models as demonstrated in the summary results shown in Table 1. Which do not alter the population probabilities but only change the coherence terms of the quantum state.

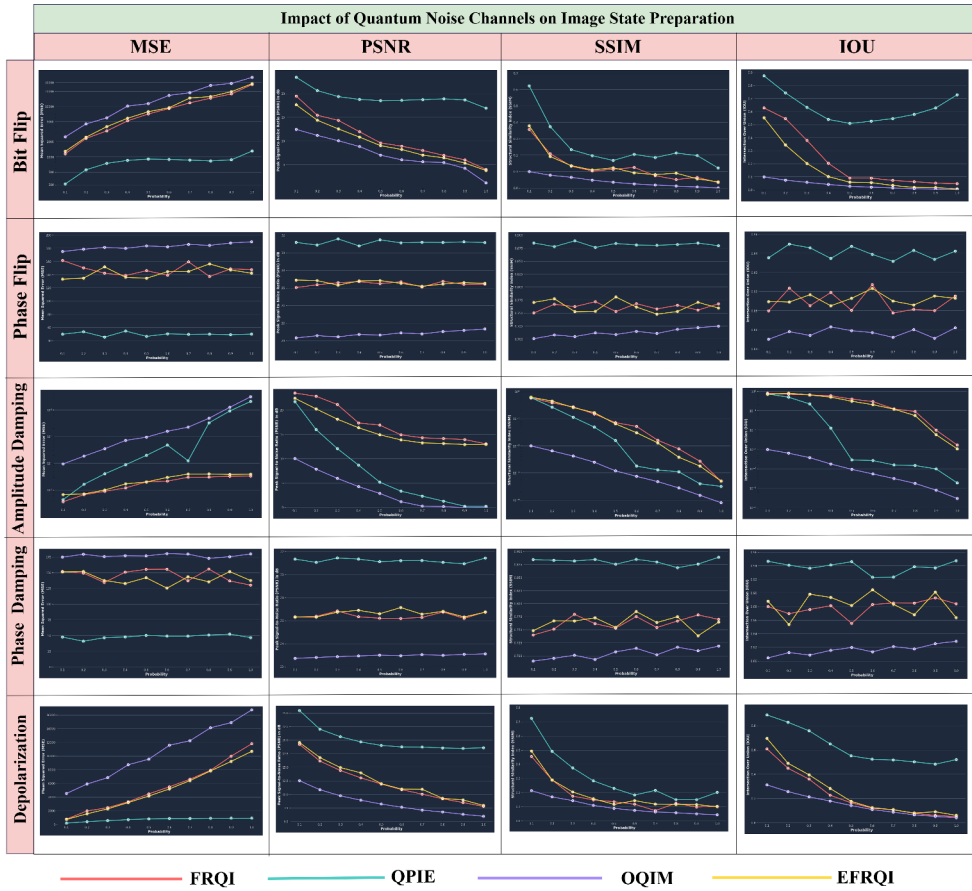


Figure 7. Quantitative results of different quantum image encoding algorithms evaluated under a noisy simulator for noise probabilities ranging from 0.1 to 1.0 across five quantum noise channels.

Consequently, the reconstructed image quality is preserved across increasing noise levels. Among the four methods, QPIE achieves slightly better metric values, whereas OQIM exhibits comparatively lower performance.

In contrast, under amplitude damping noise, FRQI and EFRQI demonstrate superior robustness compared to QPIE and OQIM. As observed in the plots, QPIE yields lower PSNR, SSIM, and IoU values than FRQI and EFRQI, although it still performs better than OQIM. This increased vulnerability of QPIE to amplitude damping arises from its encoding strategy, where pixel intensities are directly represented in the population probabilities of the quantum state. Since amplitude damping noise selectively alters population states by causing the decay of $|1\rangle$ to $|0\rangle$, the encoded intensity information in QPIE is directly degraded. In contrast, FRQI and EFRQI encode pixel information primarily in rotation angles, making their representations comparatively less sensitive to population decay effects.

Under depolarizing noise, severe degradation is observed across all encoding methods due to random Pauli errors applied along the X , Y , and Z axes. As the noise probability increases, substantial image information is lost for all methods. However, QPIE preserves a

limited amount of structural information at lower noise levels compared to the other encoding schemes, although at higher noise probabilities the reconstructed images collapse into largely random patterns.

Overall, the analysis based on both visual inspection of the reconstructed images and quantitative performance metrics demonstrates that the robustness of quantum image encoding methods strongly depends on how pixel information is mapped onto quantum states. Encoding schemes that store pixel information directly in population probabilities are more susceptible to amplitude damping noise, whereas angle- or phase-based encodings exhibit improved resilience. In contrast, FRQI and EFRQI encode grayscale information primarily through rotation angles, making them less sensitive to population decay and therefore more robust under this noise channel. Circuit complexity and qubit count further influence noise sensitivity, which accounts for the consistently lower performance of OQIM due to its higher qubit requirement and more complex encoding structure. Except for amplitude damping noise, QPIE generally preserves image information more effectively than the other methods, indicating better robustness under BF, PF, PD, and DN noise channels.

6 Conclusion

In this paper, we studied and implemented different quantum image encoding algorithms, namely FRQI, QPIE, OQIM, and EFRQI, and systematically analyzed their robustness under five quantum noise channels: bit-flip, phase-flip, amplitude damping, phase damping, and depolarizing noise. Two situations were analyzed with noise and without noise to check how the circuit performs in both the scenarios. Its incorporate with various parameters includes number of qubits needed for encoding, what type of encoding it is, the circuit depth complexity and type of preprocessing strategy. The experimental results shows that among the selected four methods QPIE consistently preserves image property in terms of structural information's and pixel wise quality in more effectively under most of the noise channels. As its performance reflected as low MSE and higher PSNR, SSIM, and IoU values. In terms of other encoding methods called FRQI and EFRQI exhibits similar comparable performance, while OQIM experiences significant loss of information degradation even at a low noise probability value ranges, primarily due to its higher qubit requirements and the circuit complexity design. Furthermore phase flip and phase damping noise channels have no disturbance with any type of selected encoding method due its property, whereas amplitude damping and depolarizing noise reduce the image quality significantly. Overall this study highlights the details depth knowledge about different perspectives of quantum image encoding techniques and underscores the importance of noise aware encoding strategies and error mitigation techniques for practical quantum image processing applications on real quantum hardware.

Acknowledgement

The first author gratefully acknowledges Vellore Institute of Technology (VIT), Vellore, for providing the financial support to carry out this research work. The computational facilities to carry out this research was supported by the Department of Science and Technology (DST), Government of India, under the FIST grant (Grant No. SR/FST/MS-II/2023/139) at VIT Vellore.

References

- [1] Ahmed, T., Kashif, M., Marchisio, A., Shafique, M. A comparative analysis and noise robustness evaluation in quantum neural networks. *Scientific Reports* **15**, 33654 (2025).

- [2] Arute, F., Arya, K., Babbush, R., Bacon, D., Bardin, J. C., Barends, R., Biswas, R., Boixo, S., Brandão, F. G., Buell, D. A., Burkett, B., et al. Quantum supremacy using a programmable superconducting processor. *Nature* **574**, 505–510 (2019).
- [3] Feynman, R. P. Simulating physics with computers. In *Feynman and Computation* (CRC Press, Boca Raton, 2018) 133–153.
- [4] Harrow, A. W., Montanaro, A. Quantum computational supremacy. *Nature* **549**, 203–209 (2017).
- [5] Khanal, B., Rivas, P. A modified depolarization approach for efficient quantum machine learning. *Mathematics* **12**, 1385 (2024).
- [6] Le, P. Q., Dong, F., Hirota, K. A flexible representation of quantum images for polynomial preparation, image compression, and processing operations. *Quantum Information Processing* **10**, 63–84 (2011).
- [7] Mitarai, K., Negoro, M., Kitagawa, M., Fujii, K. Quantum circuit learning. *Physical Review A* **98**, 032309 (2018).
- [8] Nasr, N., Younes, A., Elsayed, A. Efficient representations of digital images on quantum computers. *Multimedia Tools and Applications* **80**, 34019–34034 (2021).
- [9] Nielsen, M. A., Chuang, I. L. *Quantum Computation and Quantum Information* (Cambridge University Press, Cambridge, 2010).
- [10] Preskill, J. Quantum computing in the NISQ era and beyond. *Quantum* **2**, 79 (2018).
- [11] Tariq, N., Hamzah, R. A., Ng, T. F., Wang, S. L., Ibrahim, H. Quality assessment methods to evaluate the performance of edge detection algorithms for digital image: A systematic literature review. *IEEE Access* **9**, 87763–87776 (2021).
- [12] Winderl, D., Franco, N., Lorenz, J. M. Quantum neural networks under depolarization noise: Exploring white-box attacks and defenses. *Quantum Machine Intelligence* **6**, 83 (2024).
- [13] Xu, G., Xu, X., Wang, X., Wang, X. Order-encoded quantum image model and parallel histogram specification. *Quantum Information Processing* **18**, 11 (2019).
- [14] Yao, X. W., Wang, H., Liao, Z., Chen, M. C., Pan, J., Li, J., Zhang, K., Lin, X., Wang, Z., Luo, Z., Zheng, W. Quantum image processing and its application to edge detection: Theory and experiment. *Physical Review X* **7**, 031041 (2017).
- [15] Younes, A. Reading a single qubit system using weak measurement with variable strength. *Annals of Physics* **380**, 93–105 (2017).